Coniferous pine biomass: a novel insight into sustainable carbon materials for supercapacitors electrode

N. Manyala*, A. Bello, F. Barzegar, A. A. Khaleed, D. Y. Momodu and J. K. Dangbegnon

Department of Physics, Institute of Applied Materials, SARCHI Chair in Carbon Technology and Materials, University of Pretoria, Pretoria 0028, South Africa.

Email address: ncholu.manyala@up.ac.za (N. Manyala)

Tel: +27 (0)12 420 3549, Fax: +27 (0)12 420 2516

Highlights

• Sustainable carbon materials from pine cone biomass.
• Hydrothermal treatment of the pine cone to produce hydrochar.
• KOH activation and carbonization of the hydrochar to produce porous carbons.
• Symmetric supercapacitor based on the porous carbon exhibit good electrochemical performance.

Graphical abstract
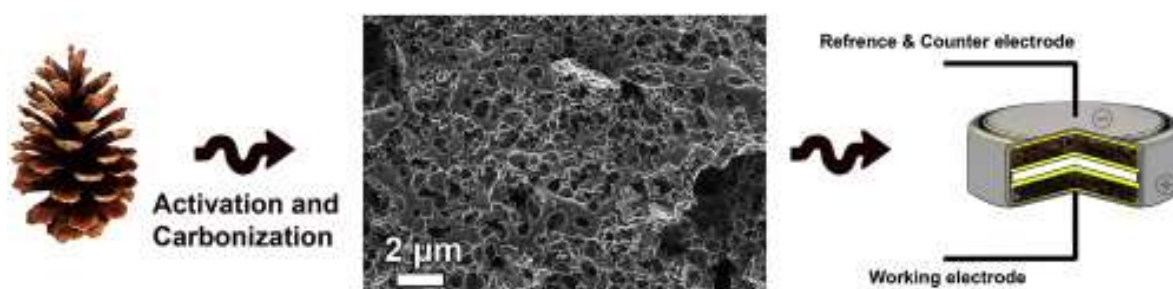
ABSTRACT

Low-cost biomass-derived activated porous carbon from natural pine cones is synthesized using hydrothermal approach followed by KOH activation and carbonization. The produced carbon materials have a high surface area of 1515 m^2 g^{-1} with a well-developed

meso/micropores structure which is advantageous and favorable for mass transfer and ion accommodation for fast rate performance by providing pathways for electrolyte permeation and contact probability. Symmetric device fabricated using the obtained carbon material as electrode, exhibited good electrochemical performance with no degradation of capacitance after voltage holding at 1 V for about 60 h demonstrating good rate capability of the fabricated device. The results demonstrate the exciting potential of the pine cone derived carbons as a promising candidate for high-performance electrode materials for supercapacitors if fully explored.

Keywords: Mesoporous material; Nanostructures; Annealing; Ageing; Electrochemical Properties

1. Introduction

Considering the increasing demand for energy and the rapid depletion of fossil fuels, the development of green and sustainable eco-friendly energy-storage systems that are highly efficient is imperative to meet the increasing energy demand for the socio-economic development of our society [1,2]. Electrochemical capacitors (ECs) also known as supercapacitors, ultracapacitors are a new class of electrochemical energy storage system which store energy by charge accumulation, and are excellent power devices that suffer from low energy density when compared with their battery counterparts which store energy using a faradaic reaction and providing high energy with moderate power [3,4]. They hold a considerable promise for a wide range of applications, including portable electronics, uninterruptable power sources, braking systems and hybrid electric vehicles [5,6]. Several

research activities are focused on improving the energy density of ECs by developing novel nanostructured electrode materials because the electrochemical performance of the electrode is highly dependent on the properties of the produce materials and electrolyte. Thus the design and optimization of nanostructured active electrode materials for the optimum balance between energy and power properties is an on-going process. To improve and achieve high energy storage capacity and high power density in ECs, carbonaceous nanomaterials such activated carbons (AC) are used to fabricate electrodes, this is because they possess nanoporous structure with high specific surface area (SSA), suitable pore size distribution, good conductivities and have high chemical stability [7,8]. Recently it has been shown that advanced form of carbon such a carbon nanotubes (CNT) [9], onion-like carbons (OLC) [10], carbide derived carbons (CDC) [6,11] and graphene [12] exhibit high capacitance, high energy and power densities as electrodes in ECs and hybrid ECs systems operating in various aqueous, organic and ionic electrolytes [6,13]. Unfortunately, the production of these advanced forms of carbon materials is significantly limited by the high cost, which is greater than the production of porous carbon derived from pyrolysis/hydrothermal treatment of biomass or bio-waste [14,15]. Hence, the need for a paradigm shift from the production of porous carbons for ECs electrodes from the conventional technique to a relatively low-cost and green carbonization approach, to meet the demand for growing global energy and sustainable development, and further to reduce the depletion of the fossil fuel raw materials [16].

Different methods like hydrothermal [17], direct pyrolysis [18], chemical vapor deposition (CVD) [19], gas-solid displacement reactions [20], and wet chemistry techniques, such as sol–gel processes [21], have been employed to produce diverse porous carbons from

biomass or waste materials such as egg shell [22], seaweeds [18], dead leaves [8], hemp basts [15], wood sawdust [17], pistachio nutshells [23], cigarette filter [24], sunflower seed shell [25], cypress [26] and rice husk [27]. Aside the low cost and sustainability benefits of these carbon-based nanomaterials they also possess high specific surface area, optimal pore size distributions, suitable average pore sizes and pathways for easy accessibility of electrolytes and rapid transportation of ions during electrochemical measurements.

In this work we have pioneered the production of porous of carbon materials from pine cone biomass as electrode for electrochemical energy storage. Pines are coniferous trees in the genus Pinus family of the Pinaceae which materialize in a wide range of environmental conditions. It sprouts up to 50 m in height with dark green needles and 5-10 cm length cones with rounded scales. Large amount of cones are produced yearly throughout the world, especially in pine plantations grown for the pulp and paper industry. They are mainly composed of cellulose, lignin and resins that contain a variety of organic compounds [28,29]. Although in the course of the literature review porous carbon from pine biomass have been studied extensively as biosorbent for metal, dye waste waters, nitrate uptake and removal of lead (II) ions from aqueous solutions by adsorption [30–32], they have never been studied as electrode for electrochemical energy storage to the best of our knowledge. Here, we report a two-step integration of hydrothermal and activation processes that uses coniferous Pines as the starting precursor for the production of porous carbons. The as-prepared products are used as the electrode materials for supercapacitors; they exhibit excellent performance with high specific capacitance of 90 F g^{-1} at the current density of 0.1 A g^{-1}, and good stability even after voltage holding for about ~3 days.

2. EXPERIMENTAL SECTION

2.1 Materials Synthesis.

The porous activated carbon powder was derived by hydrothermal process from the ground pine cones (PC) materials by a slight modification of the procedure in ref [33]. Scheme 1 shows the transformation of PC into porous carbons. PC was collected from the University of Pretoria campus Hatfield, South Africa. The cones were washed repeatedly with acetone and distilled water to remove adhering dirt and soluble impurities and dried at 60 °C. After drying, the cleaned PC was crushed and eight grams was dispersed in 80 ml of distilled water containing 0.5 ml of sulphuric acid. The dispersion was transferred into a stainless steel autoclave and was heated up to 160 °C for 12 h and then allowed to cool to room temperature. The resulting solid black product was filtered and washed with distilled water and dried overnight at 80 °C. The dried solid black product was activated using KOH with a mass ratio of 1:1. The mixture was then placed in a horizontal tube furnace ramped from room temperature to 800 °C at 10 °C/minute under argon flow and annealed for 1 hour for the carbonization process. A series of temperatures (600, 700, and 900 °C) were examined to investigate the effect of temperature on the structural evolution of the produced carbon materials. The materials were denoted as activated pine cones (APC), and APC-600, APC-700, APC-800 and APC-900 with the number denoting the carbonization temperatures.

Scheme 1. The transformation of pine cones to activated carbon.

2.2 Characterization

The samples were characterized using powder X-ray diffraction (XRD). An XPERT-PRO diffractometer (PANalytical BV, Netherlands) with theta/theta geometry, operating a cobalt tube at 35 kV and 50 mA, was used. The XRD patterns of all specimens were recorded in the 10.0° – 80.0° 2θ range with a counting time of 5.240 seconds per step. Fourier-Transform Infrared (FTIR) spectra were recorded on a Vertex 70v (Bruker) spectrometer in the 4000-600 cm^{-1} range with 4 cm^{-1} resolution and analyzed with the Opus software. Raman spectra of samples were recorded using a WiTec-alpha 300R+ confocal Raman spectrometer (WiTec GmbH) with the laser power of 1.5 mW in order to minimize heating effects. The excitation source was a 532-nm laser through a numerical aperture of 0.9 and 20x magnification. The morphologies of the activated porous carbons were observed by Zeiss Ultra Plus 55 field emission scanning electron microscope (FE-SEM) operated at an accelerating voltage of 2.0 kV. The surface area measurements of the produced samples were performed by liquid Nitrogen adsorption–desorption isotherms at −196 °C using a Micromeritics TriStar II 3020. The surface area was calculated by the Brunauer–Emmett–Teller (BET) method.

2.3 Electrochemical Performance Measurement

The electrochemical experiments were carried out using a two-electrode cell with a 1 M Na_2SO_4 aqueous electrolyte. The electrodes were prepared by mixing 80 wt.% sample, 10 wt.% carbon black and 10 wt.% Polyvinylidene fluoride (PVDF) binder in N-methylpyrrolidone (NMP) solution and pasted onto the Ni-foam current collector, which was dried at 80 °C overnight in an electric oven to ensure complete evaporation of the NMP. Each electrode has a mass loading of about 4 mg per electrode. The symmetric devices were assembled such that two electrodes were separated by a glass microfiber filter paper in

CR2025-type coin cells. The cyclic voltammetry (CV), galvanostatic charge-discharge (CD), and electrochemical impedance spectroscopy (EIS) measurements were performed on a Bio-logic VMP-300 potentiostat. CV tests were conducted between 0 and 1 V at different scan rates of 10 – 200 mV s^{-1}. The EIS plots were obtained in the frequency range from 100 kHz to 0.01 Hz at open circuit potential. The specific capacitance was calculated from the galvanostatic charge-discharge tests based on a two-electrode cell, the gravimetric specific capacitance (C$_{sp}$: F g^{-1}), the maximum energy density (E$_{max}$: Wh kg^{-1}), and the power density (P$_{max}$: kW kg^{-1}) of the cell were calculated using equations 1 to 3, respectively:

$$C_{sp} = 4 \times \text{I } \Delta t/m \, \Delta V \tag{1}$$

$$E_{max} = 0.5 \, C(\Delta V)^2 = (C_{sp} \times \Delta V^2)/28.8 \tag{2}$$

$$P_{max} = 3.6 \times E_{max}/\Delta t \tag{3}$$

where I is the discharge current (A), m is the total mass of the active material in both electrodes (g), Δt is the discharge time (s), and ΔV is the applied potential (V).

3. RESULTS AND DISCUSSION

3.1 Morphological and structural analysis

Fig. 1 show the different morphology and microstructures of the four samples prepared at different temperatures. The images clearly indicated that KOH activation process leads to the formation of porous materials. It was observed that these materials possessed the 3D open porous network architectures. Higher magnification features the existence of ample amount of pores in the 3D interconnected carbon frameworks with dimension from

nanometers to several micrometres pores in the network. The pores sizes present in the porous network ranges from meso to macropores. The primary activation reaction of materials using KOH takes place according to the following reaction;

$$6KOH + 2C \leftrightarrow 2K + 3H_2 + 2K_2CO_3$$

which is followed by decomposition of K_2CO_3 and/or reaction of K_2CO_3 with carbon [34]. The PC/KOH was annealed at different temperatures (from 600 to 900 °C) to visualise the structural evolution. The low and high magnification micrograph of the activated carbon product at 600 °C is shown in Figs. 1 (a, b). Fig. 1a shows an undulating porous surface of the material while Fig. 1b shows that the surface is quite smooth, with fewer pores and some cracks. At higher temperatures, the major alkaline species in the reactants is K_2O [35], thus increasing the annealing temperature from 700 to 900 °C (Figs. 1c - h), the PC undergoes much stronger intermolecular dehydration reactions, which induces greater structural changes leading to a much more porous network due to the release of volatiles during carbonization. At 800 °C, K_2O which melts at 740 °C could simultaneously etch carbon atoms and catalyse the removal of oxygen species. This is due to the fact that the potassium species exist in the bulk and on the surface of the PC, thus inward and outward carbonization effect will work in to convert the structure to porous morphology [34,35]. High magnification images Fig. 1 (d f and h) reveals mainly the presence of interlinked carbons with diverse porosity. Carbonization at 800 °C seems to be the best and optimum temperature as it leads to the highest specific surface area (SSA) as observed from the gas sorption which will be discussed shortly.
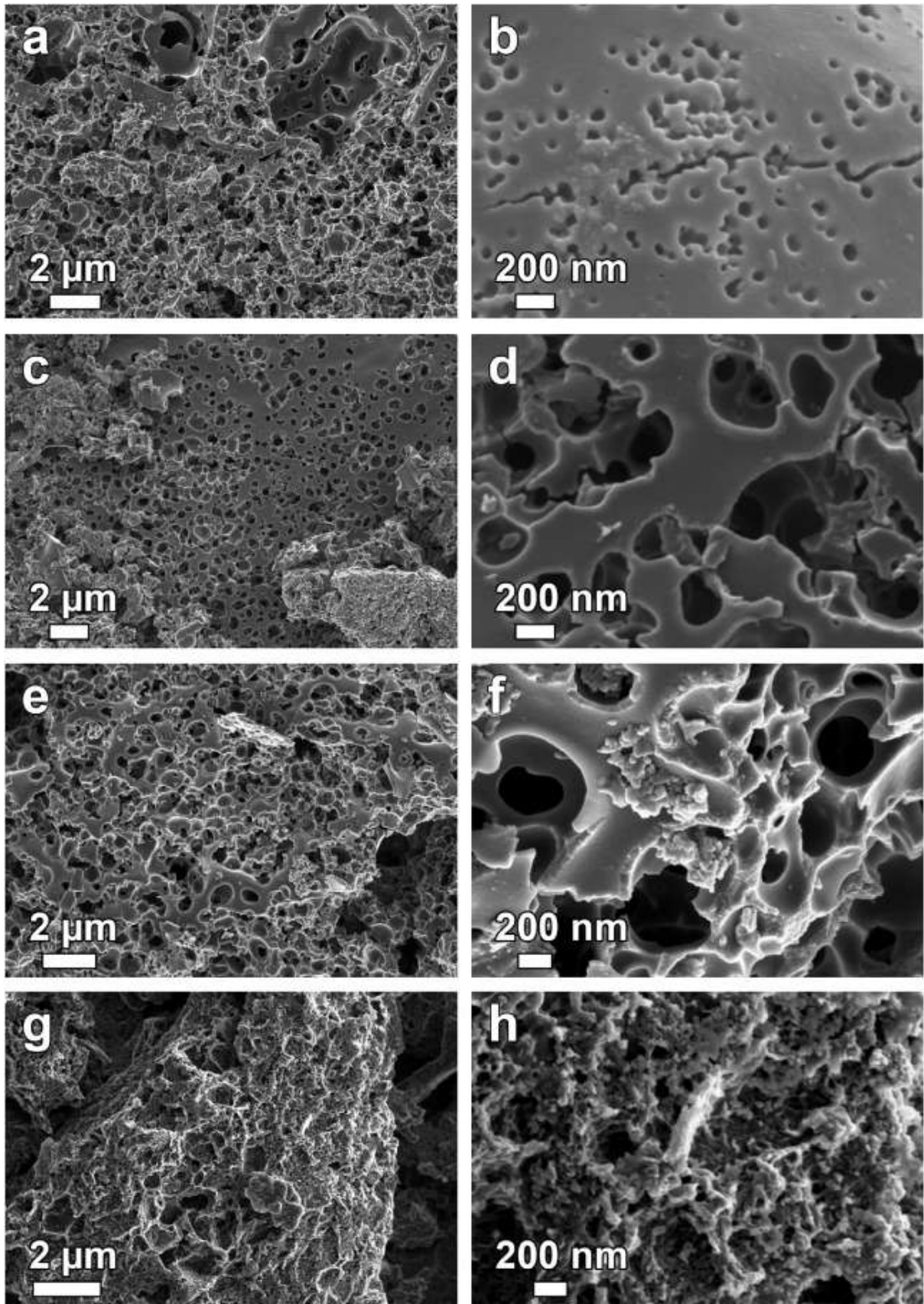
Fig. 1. SEM micrographs showing low and high magnification of (a–b) APC-600; (c–d) APC-700; (e–f) APC-800; and (g–h) APC-900.

The porous texture and structural differences of the produced APC was measured from the BET acquired from N_2 adsorption isotherms at 77 K. Fig. 2 shows that APC-600 to APC-800 exhibits the H4 Adsorption and desorption hysteresis suggesting a complex materials containing both micropores and mesopores while the APC-900 samples exhibits a type IV structural isotherms suggesting the existence of different pore sizes from micro to macropores. The obvious capillary condensation step and a hysteresis loop in the middle and high relative pressure range are indication of a typical mesoporous material. All four samples show slightly different adsorption capacities at low pressures indicating different amount of micropore volume. The specific surface area (SSA) values, the pore volume parameters extracted from Fig. 2 are presented in table 1. The sample produced at 800 °C exhibited the highest SSA and pore volumes and the smallest particle size when compared with the 600 °C and 700 °C activation temperatures. These parameters suggest that the APC-800 °C is suitable as electrode material for ECS applications. This result is in line with previous studies where it has been demonstrated that, irrespective of the precursor used, the activation of carbon using KOH can be summarized as a sequence reactions and expansion of the carbon lattice by the metallic K intercalation, giving rise to nanostructures and this occurs at about 700 °C or higher temperatures [36]. The pore size in the carbon nanosheets is mainly distributed within 2-10 nm as calculated using the BJH analysis from the adsorption branches. Fig. 2c shows the dependence of BET SSA of APC on carbonization temperature for the samples with a fixed KOH/PC hydrochar demonstrating that activation of carbon using KOH that exhibits the highest SSA occurs at a maximum temperature of about 800 °C [37]. Further increase in temperature to 900 °C led to a decrease in the SSA value and increase in pore diameter as shown in table 1. This may be due to the collapse of the porous structure during the high temperature activation process [37].
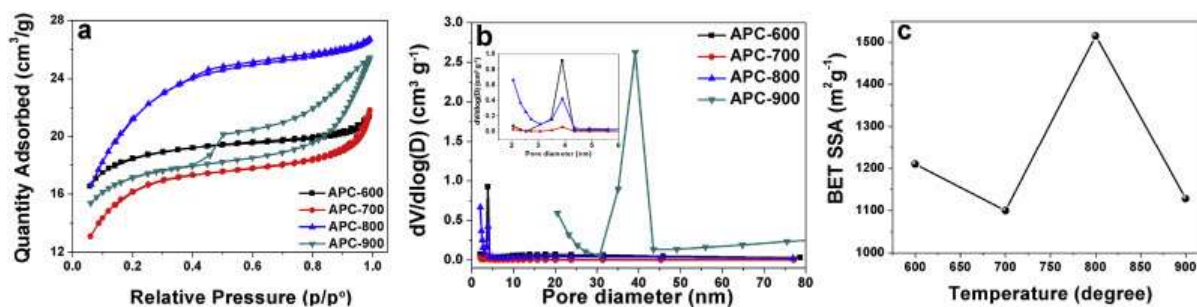
Fig. 2. (a) N_2 adsorption-desorption isotherms of APC material nanosheets; (b) Pore size distribution calculated from the adsorption isotherms using BJH method; (c) Effect of activation temperature vs. BET SSA.
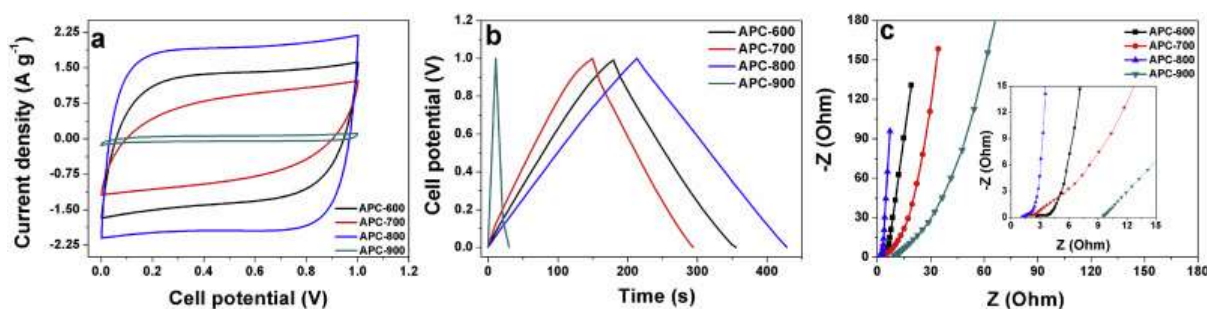

Fig. 3. Electrochemical performance of each device (a) CV curves at 100 mV s^{-1}; (b) Galvanostatic charge/discharge at 0.1 A g^{-1}; (c) Nyquist plot showing the imaginary part versus the real part of impedance for these samples.

Table 1. Physical and textural properties of porous APC materials.

Temperature	Surface area (m^2/g)	micropore volume[a] (cm^3/g)	cumulative volume[b] (cm^3/g)	Pore diameter[c] (nm)
600	1100	0.33	0.22	6.60
700	1210	0.29	0.50	5.36
800	1515	0.38	0.53	3.55
900	1128	0.36	0.45	5.07

[a] t-Plot micropore volume

[b] BJH Desorption cumulative volume of pores between 1.7000 nm and 300.0000 nm diameter

[c] BJH Desorption average pore diameter (4V/A)

The structural evolution of the APC materials as a function carbonization temperature has

been investigated by X-ray powder diffraction (XRD) and Raman spectroscopy

measurements. Fig. S1a shows the XRD comparison of all samples activated at different temperatures. All the XRD results are similar exhibiting a broad XRD peaks centred at 51°, representing the (100) diffraction plane of graphite, indicating the presence of a low degree of graphitization which suggests the carbon material exhibit extremely small "crystallite" particles that do not form crystal faces that are visible hence termed "amorphous graphitic" materials. The amorphous nature of the material could be due to corrosion effect by KOH during the thermal treatment [35]. Raman data shown in Fig.S1b displayed prominent D and G peaks in all samples located within the range of ~1345 to 1355 cm^{-1} corresponds to graphitic lattice vibration mode with A_{1g} symmetry and known to be characteristics of defect or disorder in the material and ~1582 to 1594 cm^{-1} corresponds to an ideal graphitic lattice vibrational mode with E_{2G} symmetry. The intensity of the D-band to the intensity of the G-band ($R=I_D/I_G$) of all for samples are as follows 0.97, 1.0, 0.99 and 0.98, indicates a low degree of graphitic crystalline structure [38, 39]. The Raman data was used to confirm the XRD results, and corroborating the highly disordered structure of the produced materials.

Fourier transform infrared spectroscopy (FTIR) measurements were also used to probe the surface chemistry of the samples and the details are presented in Fig. S1c - S1d of the supporting information.

3.2 Electrochemical analysis

The electrochemical behavior of the porous APC was evaluated in a symmetric two-electrode system in a 1 M Na_2SO_4 aqueous electrolyte. Fig. 3a compares the CV curves for the APC-600, APC-700, APC-800 and APC-900 electrodes at sweep rate of 100 mV s^{-1}. From these curves, the APC-600 and APC-800 devices exhibited a rectangular shape, which indicate quick ion/charge transport and predominantly electric double-layer capacitor

behavior for these materials which we attributed to the narrow porosity and micropore volume in the carbonized carbon. However the APC-700 and APC-900 exhibited low current response and distorted shape due to the slow kinetics resulting from retarded ion transport related to their structures. Fig. 3b presents the charge-discharge (CD) curves of the all devices measured at a current density of 0.1 A g^{-1} operating between 0 and 1 V. The triangular shape of the CD further confirms the non-faradaic phenomena of the devices and suggesting that these materials are suitable as electroactive materials for EDLCs applications. The CD curves of APC-800 device with a longer discharge time suggest that the electrochemical capacitances of device are higher than other samples. The higher electrochemical behaviour of the APC-800 device is ascribed to its textural properties with high SSA, high pore volume and better electronic conductivity (less presence of functional groups) as observed from the FTIR shown in the supporting information. Fig. 3c shows Nyquist plots for the four devices fabricated. The equivalent series resistance (ESR) are estimated from the horizontal position on the Nyquist in the high frequency. All devices show a nearly straight line in the low-frequency region. The symmetrical device with the APC-900 has an ESR of 9 Ω, APC-600 has an ESR of 2.5 Ω, APC-700 has an ESR of 1.5 Ω and is significantly higher than the 0.9 Ω measured with APC-800 device. The fast rate kinetics of this cell can also be explained in terms of its diffusion path length exhibiting the shortest path length as observed in Fig. 3c. Thus, indicating a nearly ideal capacitive behavior with a low diffusion resistance. From the structural properties together with the morphological characterization and electrochemical analysis, APC-800 device consistently display the best properties as electrode material for EDLCs application hence further characterization on this optimized material will be reported in this article and the electrochemical results of the other samples are presented in Fig. S2-S4 in the supporting information.
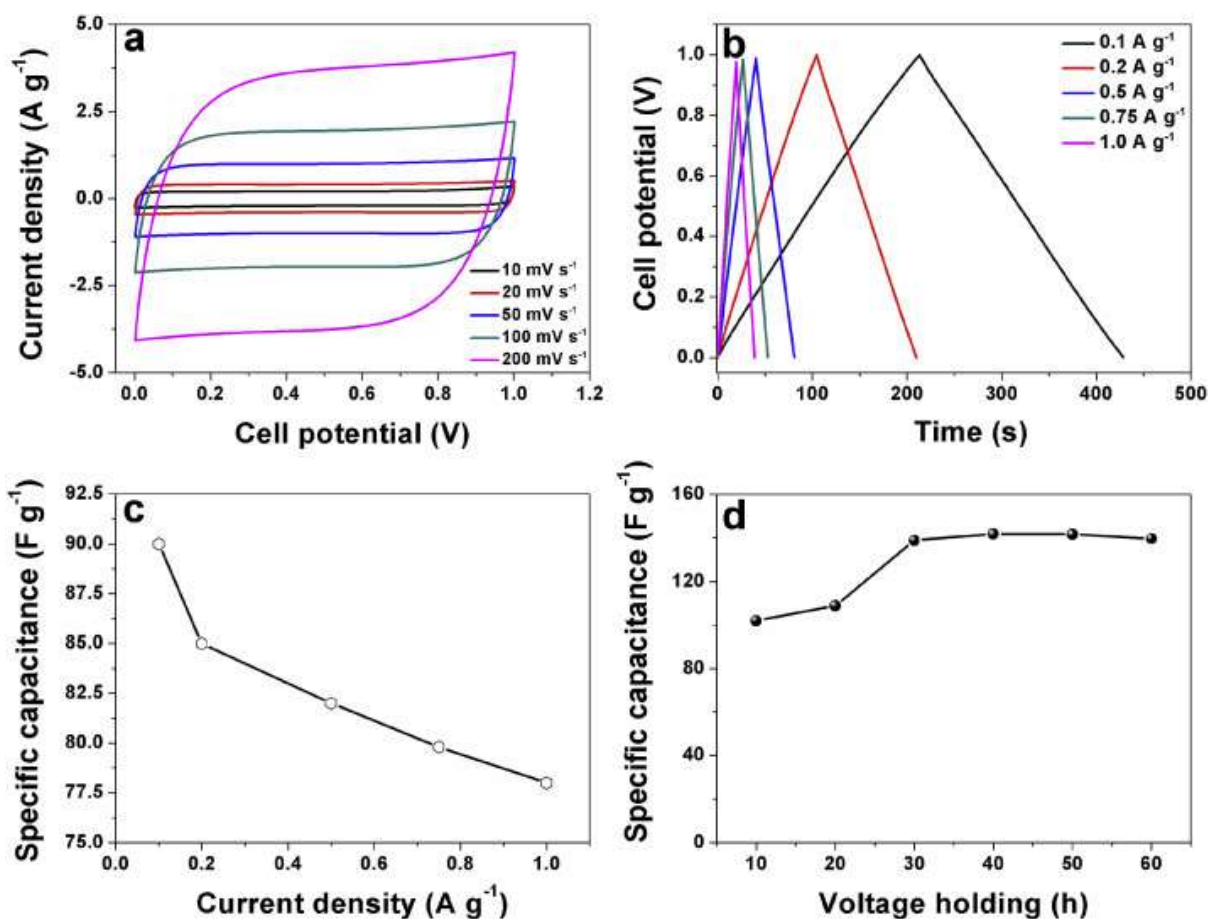
Fig. 4. Electrochemical performances tests for the APC-800 in 1 M Na_2SO_4 aqueous electrolyte at 0–1.0 V: (a) CV curves at different scan rates; (b) GCD curves at different current densities; (c) dependence of specific capacitance on discharge current density; (d) 60 h voltage holding stability test.

The CV curves for the APC-800 device at different scan rates are shown in Fig. 4a. The CV curves in Figure 4a exhibit a nearly perfect rectangular shape and with slight distortion as the scan rate increases from 10-200 mV s^{-1}, indicating a small resistance and an excellent double layers capacitive nature of this material. At 200 mV s^{-1}, the device still displays a rectangular shape, indicating ideal capacitive behavior and a very fast electrochemical response of electrodes materials, the result can be attributed to the easy movement of ions in the pores and a compact double-layer formation situation [40]. The CD profiles of the cell at various current densities is shown in Fig. 4b with symmetric triangular CD curves with no obvious ohmic drop, indicate the negligible internal resistance. The triangular shape is a

dominant indication of electric double-layer capacitor formation at the interface of electrode and electrolyte. The specific capacitances calculated from the discharge curves reduce from 90 to 78 F g^{-1} when the current density was increased from 0.1 to 1 A g^{-1}, indicating 86 % retention of the initial capacitance as shown in Fig. 4c. This suggest that the electrode allows high rate rapid ion diffusion and exhibits good electrochemical utilization when compared with previously reported porous carbons derived from biomass [24]. The energy density and power density relationship of this material is presented in Fig. S5.

Cycling test based on floating has been used to investigate the long-term stability [41]. Fig. 4d shows the stability during voltage-holding over 60 h. Floating at 1 V has a significant impact on the capacitance which slowly increases during ageing. As observed from the figure there was a rapid increase in the capacitance for the first 30 h and this capacitance was maintained for the next 30 h before starting to show slight decay. The increase in capacitance is attributed to the expansion and swelling of the porous electrode structure during the ageing time thus creating more accessible surface for adsorption of ion from the electrolyte hence increasing the capacitance of the cell. The excellent stability of the APC-800 electrode material showed that this device can be charged and discharged without notable degradation.

Electrochemical impedance spectroscopy (EIS) analysis is crucial to investigate the behavior of electrodes. The impedance measurement was taken at 5 mV sinusoidal amplitude in the frequency range of 100 kHz - 0.01 Hz. The Nyquist plot is presented in Fig. 5d featuring a partial semicircle in the high and middle frequency region indicating the presence of charge transfer resistance, and a vertical line in the low frequency indicating ideal capacitive behavior and good electronic conductivity of the APC-800 electrode material. The

intersection with the real Z' axis from Nyquist plots provides information about the ohmic resistance (R_S) which includes the total resistance of the electrolyte, intrinsic resistance of active materials and contact resistance between the active electrode material and current collector [42]. From Fig. 5a a resistance of 0.92 Ω (inset) was observed suggesting a fast ion transport and ion percolation resulting from the porous structure of the electrode material. The R_1 which corresponds to the diameter of the semicircle in the high to mid frequency region is ~ 0.3 Ω indicating an efficient charge transfer process in the electrodes. These values are comparable with other reported activated carbon electrodes from biomass [24,33,43].
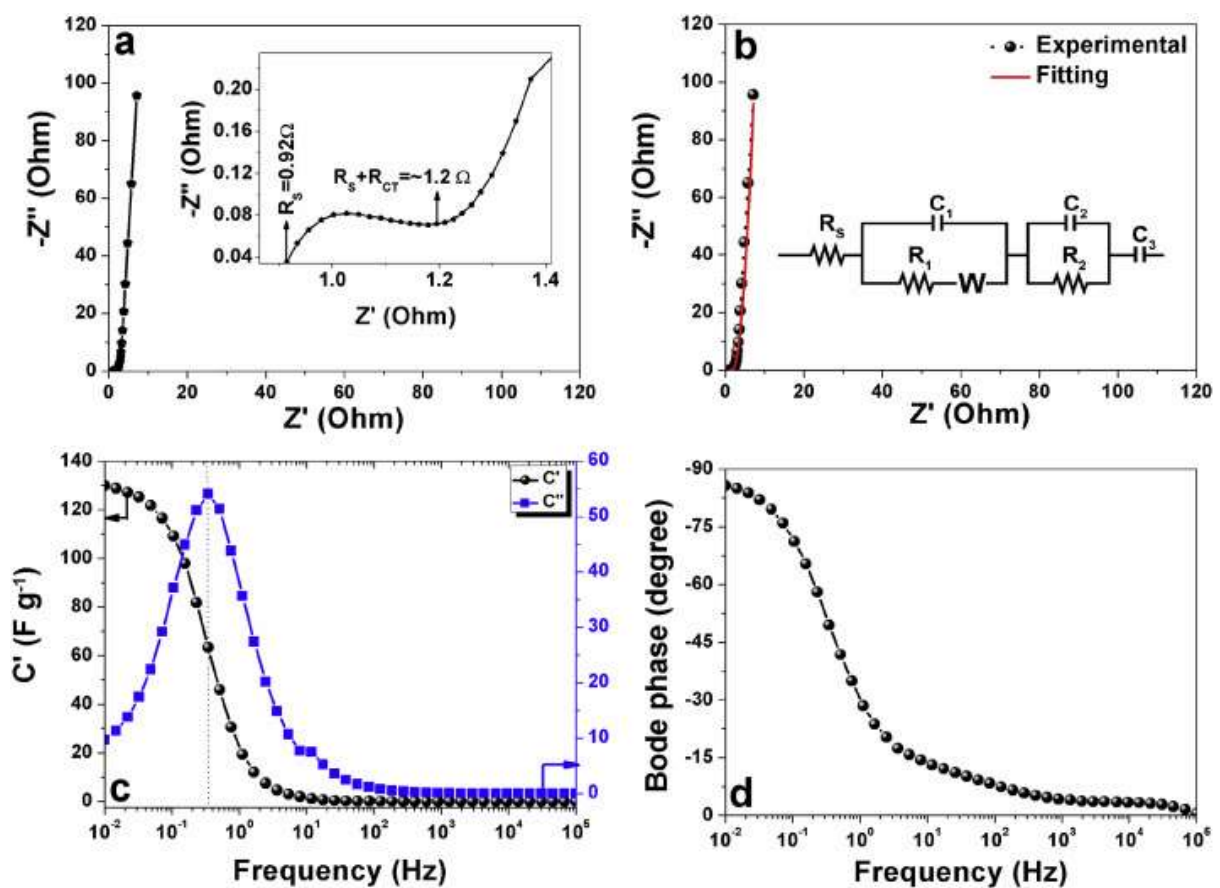

Fig. 5. (a) and (b) Nyquist plot for the APC-800 based cell in 1 M Na_2SO_4 with magnifications of the high to mid frequency region shown in the inset; and fitted with equivalent circuit shown in the inset respectively; (c) the real and imaginary part of the cell capacitance vs. frequency (black and blue curves); (d) Bode plot for the phase angle vs. frequency.

The fitting of the Nyquist plot was performed by a modified Randles circuit with a set of resistors (R) and capacitors (C) in series and parallel using ZFIT/EC-Lab program and is presented as inset to Fig. 5b [44]. As stated earlier, R_S represent the ohmic resistance of the electrolyte and the internal resistance of the porous electrode materials and the semicircle in the high to mid frequency region is presents the charge transfer resistance (R_1). From Fig. 5b the double layer capacitance of the porous material represented by C_1 is and R_1 connected parallel to each other and are in series with R_S. The transition from high to low frequency region is modelled by Warburg diffusion element (W) which is in series with the R_1. W is attributed to the diffusion of ion at low frequency and It is represented by $A/(j\omega)^{0.5}$ [45] where A is the Warburg coefficient and ω is the angular frequency. In principle, at very low frequencies, an ideal polarizable capacitive electrode would lead to a straight line parallel to imaginary axis (-Z") with a capacitance represented as C_2 in the circuit. Nonetheless, from Fig. 5b there is a divergence from this ideal behaviour. This divergence is attributed to the presence of a resistive element associated with C_2. This resistive element is referred to as leakage resistance (R_2) and is placed in parallel to C_2. C_3 is the interface contact capacitance between the porous electrode material and the current collector [46,47]. The fitting parameters are presented in table 2 and values obtained are in agreement with experimental data suggesting that model used for fitting was correct with an error of 0.042. X^2 represents the criterion for minimization of the fit. $X/\sqrt{N}$ where N is the number of points, a normalized expression of X^2, whose value is independent of the number of points and is represented as the error below.

Table 2. Fitting parameters of the Nyquist plot for the APC-800 device.

R_s	C_1	A_W	R_2	R_{CT}	C_2	C_3
(Ω)	(F)	($\Omega.s^{-0.5}$)	(Ω)	(Ω)	(F)	(F)
1.114	0.0002	1.333	0.215	0.509	0.014	0.182

$X^2 = 0.042$ $\qquad X/\sqrt{N} = 0.031$

The relaxation time constant of device and the frequency-dependent capacitance was further studied using the expression below [48]:

$$C(\omega) = \frac{1}{j\omega Z} = -\frac{Z''}{\omega|Z|^2} - j\frac{Z'}{\omega|Z|^2} = C'(\omega) + jC''(\omega) \qquad (7)$$

Where C'(ω) corresponds to the real or static capacitance which is the deliverable capacitance, C''(ω) corresponds to energy dissipation of the supercapacitor and an irreversible Faradic charge transfer process, which can cause the hysteresis of the electrochemical processes, |Z| is the impedance modulus, and ω is the angular frequency.

The capacitance from the EIS data as a function of frequency is shown in Fig. 5c. From this graph the highest specific capacitance of 130 F g^{-1} (from topmost part of the C' graph) was obtained which is slightly higher than results obtained from the CD measurements. This demonstrates the fast frequency response of the porous carbon material in aqueous solution with good capacitance, retention and high power delivery. The evolution of C'' which defines the transition frequency between a pure capacitive and a pure resistive behavior is also shown in the figure. C'' as a function of frequency shows a peak which appears at a maximum frequency of 0.35 Hz defining a relaxation time of ~2.9 s estimated from $\tau = 1/\omega_{max} = 1/(2\pi f_{max})$. This small value of τ shows how fast reaction takes place in the cell indicating that the full capacitance of the cell can be reached within a very short time. Finally, Fig. 5d shows the phase angle as a function of frequency. An ideal capacitor

has a -90° phase angle, but the presence of resistive component in the cell, especially at high frequency significantly reduces the phase angle. The plot shows that the device has a phase angle ~ -85° which is close to ideal capacitor phase angle of -90°.

4. CONCLUSION

In summary, a bio inspired porous carbon structure has been successfully prepared by employing natural pine cone materials as electrodes for electrochemical capacitors. The initial pine cones are subjected to hydrothermal treatment to obtain hydrochars, followed by KOH activation and carbonization under the argon atmosphere. The textural structure of the carbon materials exhibited a specific surface area of 1515 m^2 g^{-1} with mainly mesoporous nature. The FTIR spectra provided qualitative information about the surface functional groups present in the produced materials. Symmetric supercapacitor devices fabricated suggests that the porous characteristics of these materials can provide efficient ion transport during electrochemical measurements. The obtained results are quite interesting, encouraging and showed the applicability of pine cones derived carbons, demonstrating the exciting potential for a low-cost porous carbon which could be ideal for use as electrodes for supercapacitor. Taking into account the worldwide abundance, availability and recyclability of pine cones, especially in plantation areas they could act as a new biomass source for production of porous carbon materials for high-performance supercapacitors. We conclude that further exploration of pine cone derived carbons as a supercapacitor electrode fully optimized and further increase in the capacitance is warranted in the field of energy storage technology. This can be achieved through optimization of the electrode design, rational selection of the electrolyte with either ionic,

organic or polymer gel electrolyte, which would increase the cell's operating potential window and the use of an asymmetric device configuration.

ACKNOWLEDGEMENT

REFERENCES

[1]   L. Li, S.-H. Chai, S. Dai, A. Manthiram, Advanced hybrid Li-air batteries with high-performance mesoporous nanocatalysts, Energy Environ. Sci. 7 (2014) 2630–2636.

[2]   H. Jiang, P.S. Lee, C. Li, 3D carbon based nanostructures for advanced supercapacitors, Energy Environ. Sci. 6 (2013) 41–53.

[3]   J.R. Miller, P. Simon, Electrochemical capacitors for energy management, Sci. Mag. 321 (2008) 651–652.

[4]   P. Simon, Y. Gogotsi, B. Dunn, Where do batteries end and supercapacitors begin?, Sci. Mag. 343 (2014) pp–1210.

[5]   B.E. Conway, Electrochemical Supercapacitors Scientific Fundamentals and Technological Applications, Kluwer Academic/Plenum: New York, 1999.

[6]   P. Simon, Y. Gogotsi, Materials for electrochemical capacitors, Nat. Mater. 7 (2008) 845–854.

[7]   M. Sevilla, A.B. Fuertes, Direct Synthesis of Highly Porous Interconnected Carbon Nanosheets and Their Application as High-Performance Supercapacitors, ACS Nano. 8 (2014) 5069–5078.

[8]   M. Biswal, A. Banerjee, M. Deo, S. Ogale, From dead leaves to high energy density supercapacitors, Energy Environ. Sci. 6 (2013) 1249–1259.

[9]   D.N. Futaba, K. Hata, T. Yamada, T. Hiraoka, Y. Hayamizu, Y. Kakudate, O. Tanaike, H. Hatori, M. Yumura, S. Iijima, Shape-engineerable and highly densely packed single-walled carbon nanotubes and their application as super-capacitor electrodes, Nat. Mater. 5 (2006) 987–994.

[10]   P. Simon, Y. Gogotsi, Capacitive energy storage in nanostructured carbon-electrolyte systems, Acc. Chem. Res. 46 (2012) 1094–1103.

[11]   Y. Korenblit, M. Rose, E. Kockrick, L. Borchardt, A. Kvit, S. Kaskel, G. Yushin, High-rate electrochemical capacitors based on ordered mesoporous silicon carbide-derived carbon, ACS Nano. 4 (2010) 1337–1344.

[12]   L.L. Zhang, R. Zhou, X.S. Zhao, Graphene-based materials as supercapacitor electrodes, J. Mater. Chem. 20 (2010) 5983–5992.

[13]   L.L. Zhang, X.S. Zhao, Carbon-based materials as supercapacitor electrodes., Chem. Soc. Rev. 38 (2009) 2520–31.

[14]   L. Wei, G. Yushin, Nanostructured activated carbons from natural precursors for electrical double layer capacitors, Nano Energy. 1 (2012) 552–565.

[15]   H. Wang, Z. Xu, A. Kohandehghan, Z. Li, K. Cui, X. Tan, T. J. Stephenson, C. K. King'ondu, C. M. B. Holt, B. C. Olsen, J. K. Tak, D. Harfield, A. O. Anyia, D. Mitlin, Interconnected carbon nanosheets derived from hemp for ultrafast supercapacitors with high energy, ACS Nano. 7 (2013) 5131–5141.

[16]   P.T. Anastas, J.C. Warner, Green chemistry: theory and practice, Oxford university press, 2000.

[17]   L. Wei, M. Sevilla, A.B. Fuertes, R. Mokaya, G. Yushin, Hydrothermal Carbonization of Abundant Renewable Natural Organic Chemicals for High-Performance Supercapacitor Electrodes, Adv. Energy Mater. 1 (2011) 356–361.

[18]   E. Raymundo-Piñero, M. Cadek, F. Béguin, Tuning Carbon Materials for Supercapacitors by Direct Pyrolysis of Seaweeds, Adv. Funct. Mater. 19 (2009) 1032–1039.

[19]   A.R. Mohamed, M. Mohammadi, G.N. Darzi, Preparation of carbon molecular sieve from lignocellulosic biomass: A review, Renew. Sustain. Energy Rev. 14 (2010) 1591–1599.

[20]   D. Vamvuka, Bio-oil, solid and gaseous biofuels from biomass pyrolysis processes—An overview, Int. J. Energy Res. 35 (2011) 835–862.

[21]   Y. Qu, Y. Tian, B. Zou, J. Zhang, Y. Zheng, L. Wang, Y. Li, C. Rong, Z. Wang, A novel mesoporous lignin/silica hybrid from rice husk produced by a sol-gel method, Bioresour. Technol. 101 (2010) 8402–8405.

[22]   H. Tang, P. Gao, X. Liu, H. Zhu, Z. Bao, Bio-derived calcite as a sustainable source for graphene as high-performance electrode material for energy storage, J. Mater. Chem. A. 2 (2014) 15734–15739.

[23]   J. Xu, Q. Gao, Y. Zhang, Y. Tan, W. Tian, L. Zhu, L. Jiang, Preparing two-dimensional microporous carbon from Pistachio nutshell with high areal capacitance as supercapacitor materials, Sci. Rep. 4 (2014).

[24]   M. Lee, G.-P. Kim, H.D. Song, S. Park, J. Yi, Preparation of energy storage material derived from a used cigarette filter for a supercapacitor electrode, Nanotechnology. 25 (2014) 345601.

[25]   X. Li, W. Xing, S. Zhuo, J. Zhou, F. Li, S.-Z. Qiao, G.-Q. Lu, Preparation of capacitor's electrode from sunflower seed shell, Bioresour. Technol. 102 (2011) 1118–1123.

[26]   E. Ito, S. Mozia, M. Okuda, T. Nakano, M. Toyoda, M. Inagaki, Nanoporous carbons from cypress II. Application to electric double layer capacitors, New Carbon Mater. 22 (2007) 321–326.

[27]   S. Kumagai, M. Sato, D. Tashima, Electrical double-layer capacitance of micro-and mesoporous activated carbon prepared from rice husk and beet sugar, Electrochim. Acta. 114 (2013) 617–626.

[28]   N. Ayrilmis, U. Buyuksari, E. Avci, E. Koc, Utilization of pine (Pinus pinea L.) cone in manufacture of wood based composite, For. Ecol. Manage. 259 (2009) 65–70.

[29]   J.A. Micales, J.S. Han, J.L. Davis, R.A. Young, Chemical composition and fungitoxic activities of pine cone extractives, in: Mycotoxins, Wood Decay, Plant Stress. Biocorrosion, Gen. Biodeterior., Springer, 1994: pp. 317–332.

[30]   G. V Nunell, M.E. Fernandez, P.R. Bonelli, A.L. Cukierman, Nitrate uptake improvement by modified activated carbons developed from two species of pine cones, J. Colloid Interface Sci. 440 (2015) 102–108.

[31]   A.E. Ofomaja, E.B. Naidoo, Biosorption of copper from aqueous solution by chemically activated pine cone: a kinetic study, Chem. Eng. J. 175 (2011) 260–270.

[32]   A. Özhan, Ö. Sahin, M.M. Küçük, C. Saka, Preparation and characterization of activated carbon from pine cone by microwave-induced ZnCl2 activation and its effects on the adsorption of methylene blue, Cellulose. 21 (2014) 2457–2467.

[33]   W. Tian, Q. Gao, Y. Tan, K. Yang, L. Zhu, C. Yang, et al., Bio-inspired beehive-like hierarchical nanoporous carbon derived from bamboo-based industrial by-product as a high performance supercapacitor electrode material, J. Mater. Chem. A. 3 (2015) 5656–5664.

[34]   J. Wang, S. Kaskel, KOH activation of carbon-based materials for energy storage, J. Mater. Chem. 22 (2012) 23710–23725.

[35]   X. Zheng, W. Lv, Y. Tao, J. Shao, C. Zhang, D. Liu, J. Luo, D.-W. Wang, Q.-H. Yang, Oriented and Interlinked Porous Carbon Nanosheets with an Extraordinary Capacitive Performance, Chem. Mater. 26 (2014) 6896–6903.

[36]   M. Molina-Sabio, F. Rodriguez-Reinoso, Role of chemical activation in the development of carbon porosity, Colloids Surfaces A Physicochem. Eng. Asp. 241 (2004) 15–25.

[37] S. Murali, J.R. Potts, S. Stoller, J. Park, M.D. Stoller, L.L. Zhang, Y. Zhu, R. S. Ruoff, Preparation of activated graphene and effect of activation parameters on electrochemical capacitance, Carbon 50 (2012) 3482–3485.

[38] W. Gao, L.B. Alemany, L. Ci, P.M. Ajayan, New insights into the structure and reduction of graphite oxide, Nat. Chem. 1 (2009) 403–408.

[39] M. Momčilović, M. Purenović, A. Bojić, A. Zarubica, M. Randjelović, Removal of lead (II) ions from aqueous solutions by adsorption onto pine cone activated carbon, Desalination. 276 (2011) 53–59.

[40] Y. Liang, F. Liang, H. Zhong, Z. Li, R. Fu, D. Wu, An advanced carbonaceous porous network for high-performance organic electrolyte supercapacitors, J. Mater. Chem. A. 1 (2013) 7000–7005.

[41] P. Ratajczak, K. Jurewicz, F. Béguin, Factors contributing to ageing of high voltage carbon/carbon supercapacitors in salt aqueous electrolyte, J. Appl. Electrochem. 44 (2014) 475–480.

[42] J. Luo, H.D. Jang, J. Huang, Effect of sheet morphology on the scalability of graphene-based ultracapacitors, ACS Nano. 7 (2013) 1464–1471.

[43] C. Peng, J. Lang, S. Xu, X. Wang, Oxygen-enriched activated carbons from pomelo peel in high energy density supercapacitors, RSC Adv. 4 (2014) 54662–54667.

[44] J.E.B. Randles, Kinetics of rapid electrode reactions, Discuss. Faraday Soc. 1 (1947) 11–19.

[45] H. Li, J. Wang, Q. Chu, Z. Wang, F. Zhang, S. Wang, Theoretical and experimental specific capacitance of polyaniline in sulfuric acid, J. Power Sources. 190 (2009) 578–586.

[46] C. Masarapu, H.F. Zeng, K.H. Hung, B. Wei, Effect of temperature on the capacitance of carbon nanotube supercapacitors, ACS Nano. 3 (2009) 2199–2206.

[47] Y. Zhou, H. Xu, N. Lachman, M. Ghaffari, S. Wu, Y. Liu, A. Ugur, K. K. Gleason, B. L. Wardle, Q.M. Zhang, Advanced asymmetric supercapacitor based on conducting polymer and aligned carbon nanotubes with controlled nanomorphology, Nano Energy. 9 (2014) 176–185.

[48] P.L. Taberna, P. Simon, J.-F. Fauvarque, Electrochemical characteristics and impedance spectroscopy studies of carbon-carbon supercapacitors, J. Electrochem. Soc. 150 (2003) A292–A300.

Supporting information

Figure S1c show the spectra of the raw pine before (black curve) and that of the sample, after hydrothermal treatment (red curve). A broad absorption band at ~3000-3600 cm^{-1} with a maximum at about 3354.9 cm^{-1} is assigned to O–H stretching vibration of the surface hydroxyl groups, while the band at ~ 2958.90 cm^{-1} shows the presence of aliphatic group (C-H) and the peak at 1647.08 cm^{-1} represents C=O stretching vibrations of ketones, aldehydes, lactones or carboxyl groups. Peaks observed between 1100.81 and 559.32 cm^{-1} may be assigned to the -C-C-and -CN stretching [1]. The red curve shows the FTIR after hydrothermal treatment, similar peaks were observed with enhanced intensity and magnitude. Fig. S1 (d) shows the FTIR spectra of the pine cone after carbonization. It is obvious that surface hydroxyl groups existed on the surface of all the produced carbon material at different temperatures. Similar absorption bands were observed with disappearance of some peak after carbonization. For example the band at 3354.9 cm^{-1} due to (O-H) stretching is no longer visible with increasing temperature from 600-900 °C. This is due to the fact that higher temperatures could lead to the breaking of the bonds of the carboxylic groups and evaporate them as volatile matter. The very weak band at 2650 cm^{-1} represents the asymmetric vibration of -CH$_2$ group [2]. Further increase in temperature progressively diminishes the intensity of the vibrational mode as observed in the figure. At 900 °C the FTIR spectrum with no visible band could be observed suggesting that this temperature could be too high for this type of biomass material and thus the drop in surface area as observed from the gas sorption analysis. This could drastically affect the performance of devices made from material carbonized at 900 °C.
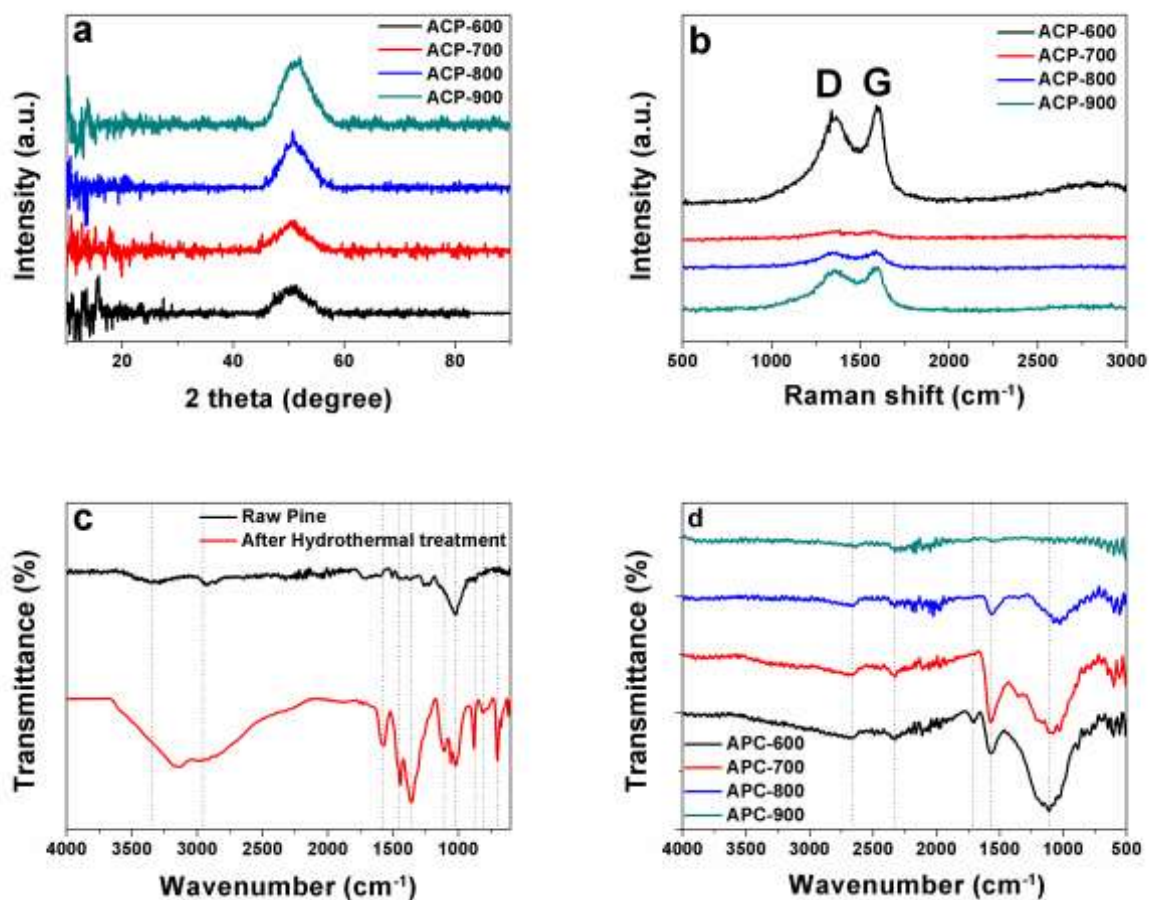
Figure S1. (a) XRD pattern of as-syntheisized ACP materials at different temperatures showing broad peak at 51° (b) Raman spectroscopy showing prominent D and G peaks in all samples; (c)FTIR spectra of raw and hydrothermal treated pine; (d) FTIR of the carbonized pine cone powder.
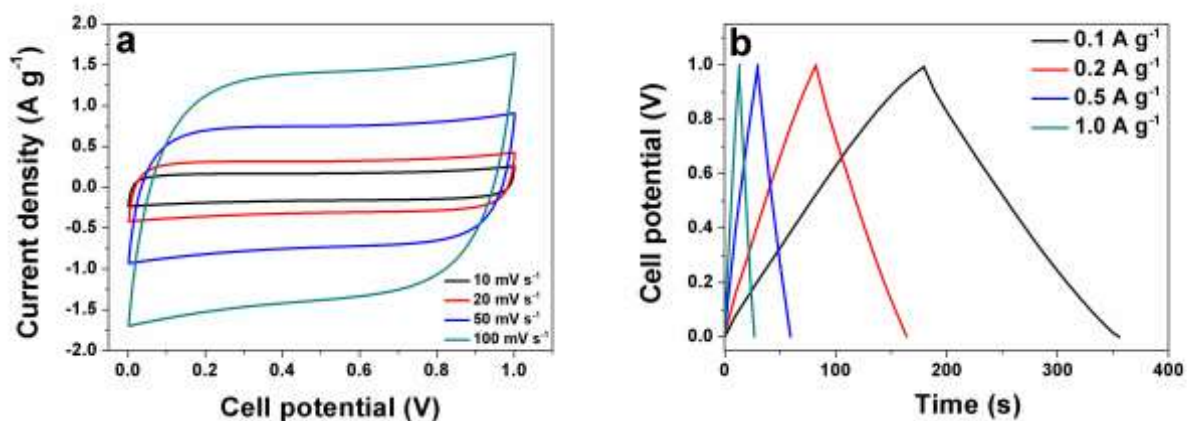

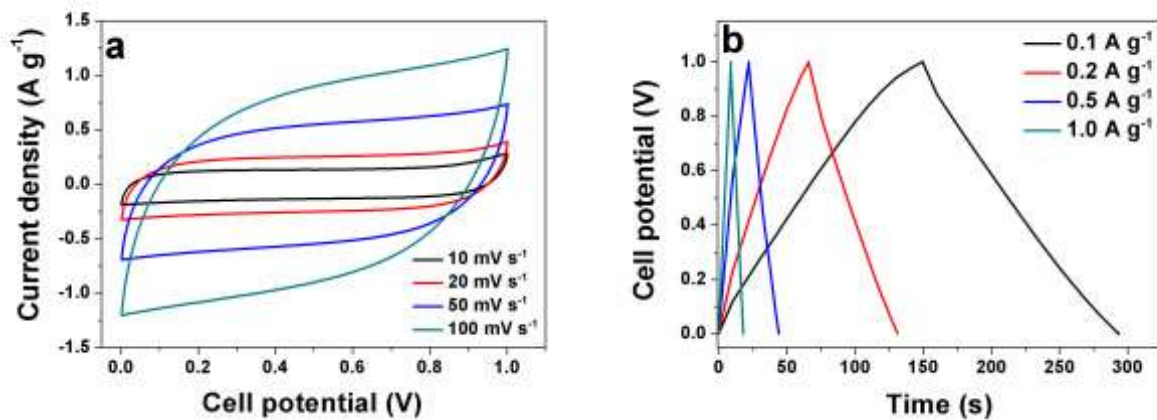**Figure S2.** CV at different scan rate and CD at differen current density of APC-600.

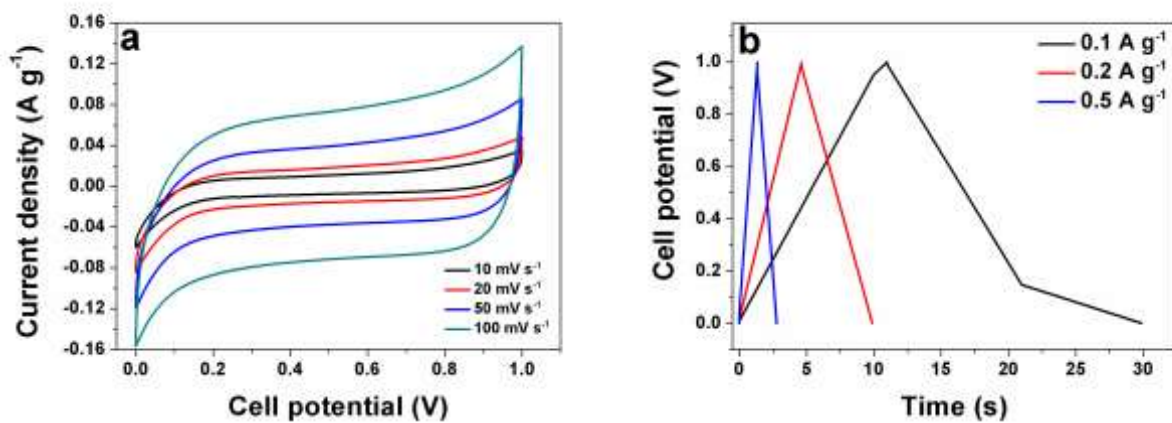**Figure S3.** CV at different scan rate and CD at differen current density of APC-700.

Figure S4. CV at different scan rate and CD at differen current density of APC-900.
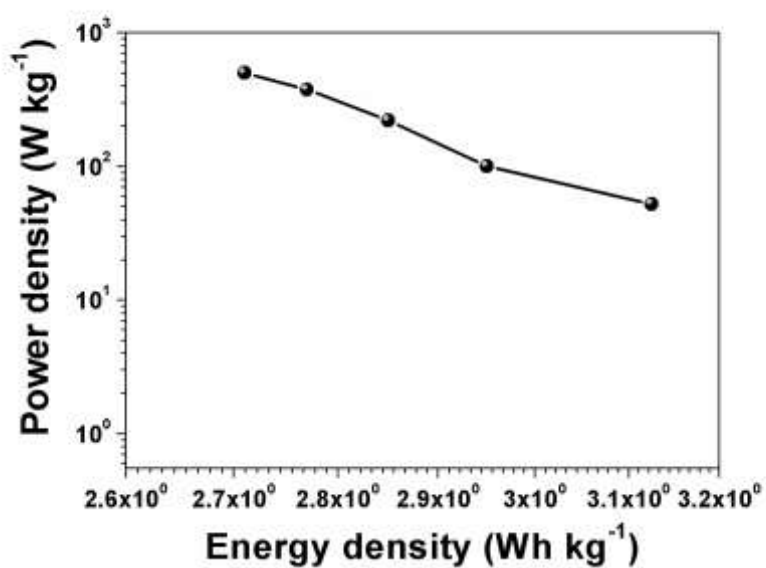
Figure S5. Ragone plot of APC-800 device

References

[1]   A.E. Ofomaja, E.B. Naidoo, Biosorption of copper from aqueous solution by chemically activated pine cone: a kinetic study, Chem. Eng. J. 175 (2011) 260–270.

[2]   M. Momčilović, M. Purenović, A. Bojić, A. Zarubica, M. Randjelović, Removal of lead (II) ions from aqueous solutions by adsorption onto pine cone activated carbon, Desalination. 276 (2011) 53–59.